

Bismuth Pyromanganate: Hydrothermal and Solid State Synthesis, Characterization and Optical Properties

SH. Khademinia^a, M. Behzad^{a,*}

^a Department of Chemistry, Semnan University, Semnan, Iran.

ARTICLE INFO

Article history:

Received 27 September 2014

Accepted 05 December 2014

Available online 15 March 2015

Keywords:

Bi₂Mn₂O₇

Hydrothermal method

Solid state

Nano materials

PXRD

ABSTRACT

Bi₂Mn₂O₇ nano-powders were synthesized via hydrothermal method involving stoichiometric 1:1 Bi to Mn molar ratio at 180°C for 48 h in a 1M NaOH aqueous solution, and solid state method, using Bi(NO₃)₃.5H₂O and MnO₂ as raw materials. The synthesized materials were characterized by powder X-ray diffraction (PXRD) technique. Also, the Rietveld analysis was performed in FullProf in profile matching mode. It was found that Bi₂Mn₂O₇ crystallizes in a cubic crystal structure with space group **Fd $\bar{3}$ m**. The size and morphologies of the synthesized materials were studied by transmission electron microscopy (TEM) and field emission scanning electron microscopy (FESEM), respectively. Also, BET-BJH analysis was carried out for determination of pore size, pore volume, average particle size, pore width and surface area of the obtained materials. Also, photoluminescence spectra of the obtained materials were studied. The FESEM images showed that the synthesized Bi₂Mn₂O₇ has rod-like structure in hydrothermal method and a mixture of rod and particle structures in solid state method.

1. Introduction

Oxides and fluorites with the general formula of A₂B₂O₇ (where A is a medium-large cation and B is an octahedrally coordinated, high-charge cation) have been widely studied for their technological potential owing to their ferroelectric and/or magnetic, ionic conductors, catalysts, phosphors, radiation resistant properties [1-5]. Pyrochlore materials have attracted great interest due to their ability to form substituted and defective structures, permitting interesting physical properties [6]. Bi₂Mn₂O₇ has already been prepared by a conventional solid state reaction method [7] and has been reported to

have catalytic ability for oxygen reduction [8]. The unit cell of this structure is usually face centered cubic with space group **Fd $\bar{3}$ m** with eight molecules per unit cell (Z = 8) [9]. In the present study, a hydrothermal route was employed to synthesize nanostructured Bi₂Mn₂O₇ powders using Bi(NO₃)₃.5H₂O, MnO₂ and NaOH for the first time. A solid state synthesis in a system of Bi(NO₃)₃.5H₂O, MnO₂ was also achieved. To the best of our knowledge, there is no report on the synthesis of nanostructured Bi₂Mn₂O₇ by these methods. BET-BJH analyses and photoluminescence spectra of the obtained materials were also studied.

Corresponding author:

E-mail address: mbehzad@semnan.ac.ir (Shahin Khademinia).

2. Experimental

All chemicals including $\text{Bi}(\text{NO}_3)_3 \cdot 5\text{H}_2\text{O}$, MnO_2 and NaOH were of analytical grade and were obtained from commercial sources (Merck Company) and used without further purifications. The materials S_1 and S_2 were synthesized via hydrothermal and solid state methods, respectively. Phase identifications were performed on a powder X-ray diffractometer D5000 (Siemens AG, Germany) using $\text{Cu-K}\alpha$ radiation. The morphology of the obtained materials was examined with by field emission scanning electron microscopy (Hitachi FE-SEM S-4160). Photoluminescence spectra were recorded on a Perkin Elmer LF-5 spectrometer (PerkinElmer Inc., Waltham, USA). The surface area and pore volume and average nanoparticles size were calculated using the Brunauer-Emmett-Teller (BET) equation. Pore size distributions, pore volume and pore surface area were calculated by the Barrett-Joyner-Halenda (BJH) method. BET surface areas were acquired on a Beckman Coulter SA3100 surface area analyzer. The rietveld analysis was carried out in FullProf with a χ^2 of 6.7 in profile matching mode.

2. 1. Hydrothermal and solid state synthesis of $\text{Bi}_2\text{Mn}_2\text{O}_7$

In typical synthetic experiments in both methods, 1.00 g (2.06 mmol) of $\text{Bi}(\text{NO}_3)_3 \cdot 5\text{H}_2\text{O}$ ($\text{Mw} = 485.07 \text{ g mol}^{-1}$) and 0.18 g (2.06 mmol) of MnO_2 ($\text{Mw} = 86.94 \text{ g mol}^{-1}$) were used. In hydrothermal method, the raw materials were added to 70 mL of hot aqueous solutions of 1M NaOH under magnetic stirring at 80°C . The resultant solution was stirred for further 15 min and transferred to a 100-mL Teflon lined stainless steel autoclave. The autoclave was sealed and heated at 180°C for 48 h. When the reaction was completed, it was immediately cooled down to room temperature by water. The prepared powder was washed with distilled water and dried at 110°C for 20 min under normal atmospheric conditions and a cream - white powder was collected. In the solid state synthesis, the raw materials were added to a 25 mL crucible and treated at 550°C for 8h. Then the product was normally cooled down to room temperature in the oven. The obtained

powder was collected for further analyses.

3. Result and discussion

3. 1. Powder X-ray diffraction analysis

The X-ray diffraction patterns of the $\text{Bi}_2\text{Mn}_2\text{O}_7$ samples are reported in fig. 1 (a and b) as data points, together with the result of the profile matching analysis (full lines). Fig. 1a shows the X-ray diffraction (XRD) pattern of the $\text{Bi}_2\text{Mn}_2\text{O}_7$ sample obtained in the θ -2 θ geometry with $\text{Cu-K}\alpha$ radiation. Structural analysis was performed through the FullProf program by employing profile matching with constant scale factor. The pattern in fig. 1 (a, b) is typical of a cubic structure $\text{Bi}_2\text{Mn}_2\text{O}_7$, reported with space group of $\text{Fd}\bar{3}\text{m}$. The red bars are the observed intensities which were obtained from the diffraction data. The black ones are the calculated data, and the blue one is the difference: $Y_{\text{obs}} - Y_{\text{calc}}$. The bars below indicate the Bragg reflections. Since we have two lines of bars, it means that we have two phases. The upper one is $\text{Bi}_2\text{Mn}_2\text{O}_7$ and the lower one shows the Bi_2O_3 reflections. The results demonstrate that the pattern has a main $\text{Bi}_2\text{Mn}_2\text{O}_7$ crystal structure with space group of $\text{Fd}\bar{3}\text{m}$. The Bi_2O_3 structure is detected with a space group of $\text{P}2_1/\text{c}$. Bi_2O_3 lattice parameters are found as $a = 5.842770 \text{ \AA}$, $b = 8.147644 \text{ \AA}$, and $c = 7.498813 \text{ \AA}$ with $\alpha = \gamma = 90^\circ, \beta = 113.024^\circ$.

Fig. 1b shows that by changing the synthesis method to solid state, there is a mixture of three phases including $\text{Bi}_2\text{Mn}_2\text{O}_7$ as a main phase, Bi_2O_3 and Mn_2O_3 with space group of $\text{Ia}\bar{3}$. The results show that the pattern has a main $\text{Bi}_2\text{Mn}_2\text{O}_7$ crystal structure with space group of $\text{Fd}\bar{3}\text{m}$. The Bi_2O_3 structure is detected with a space group of $\text{P}2_1/\text{c}$. Bi_2O_3 lattice parameters are found as $a = 5.850432 \text{ \AA}$, $b = 8.290177 \text{ \AA}$, and $c = 7.555346 \text{ \AA}$ with $\alpha = \gamma = 90^\circ, \beta = 113.158^\circ$. The Mn_2O_3 structure is detected with a space group of $\text{Ia}\bar{3}$. The Mn_2O_3 lattice parameters are found as $a = b = c = 10.672101 \text{ \AA}$.

The measured powder XRD data are in agreement with those of reported XRD for $\text{Bi}_2\text{Mn}_2\text{O}_7$ nanomaterials [7, 8]. In view of

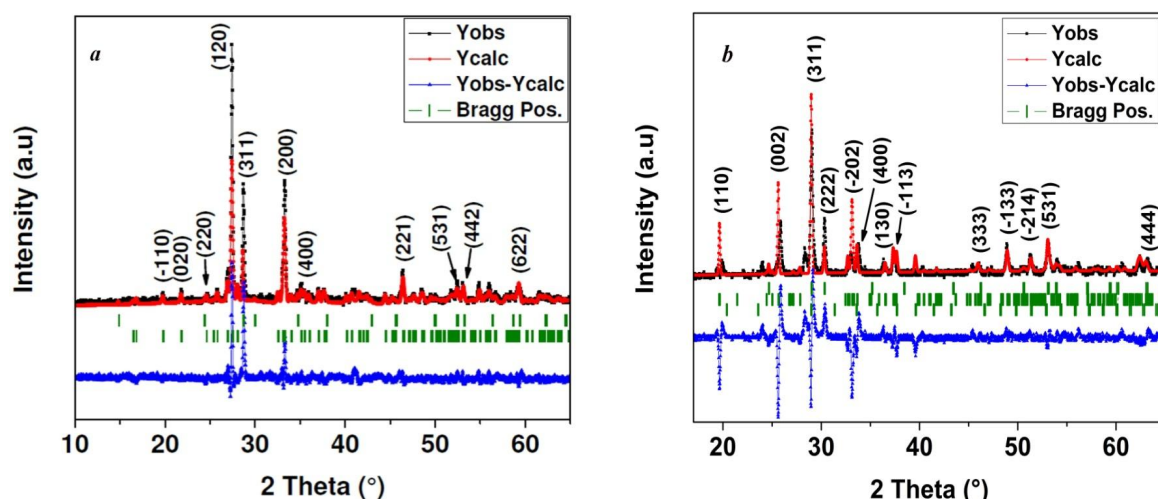


Fig. 1. PXRD patterns of the a) hydrothermally and b) solid state synthesized $\text{Bi}_2\text{Mn}_2\text{O}_7$ nanomaterials

theoretical calculations, pyrochlore oxides are found to be stable when the radius ratio (r_A/r_B) of the cations lies in the range of 1.46–1.78. Oxides of general formula $\text{A}_2\text{B}_2\text{O}_7$ crystallize in ordered pyrochlore (cubic, $\text{Fd}\bar{3}\text{m}$) and defect fluorite (cubic, $\text{Fm}\bar{3}\text{m}$) structures when the radius ratio (r_A/r_B) is in the upper or lower limits of the above range. In the present investigation, the radius ratio (r_A/r_B) for $\text{Bi}_2\text{Mn}_2\text{O}_7$ is higher than 1.78 and the obtained stable phase is isostructural with $\text{Bi}_2\text{Mn}_2\text{O}_7$ (space group $\text{Fd}\bar{3}\text{m}$) (radius of Bi^{3+} cations is about 1.17\AA and Mn^{4+} 0.53\AA) [10-13], which is in agreement with the Rietveld analysis data. Compared to the nanomaterials of the hydrothermally synthesized $\text{Bi}_2\text{Mn}_2\text{O}_7$ (S_1), the diffraction lines in the powder XRD patterns of the solid state synthesized $\text{Bi}_2\text{Mn}_2\text{O}_7$ (S_2) nanomaterials has shifted to lower 2θ values and therefore to higher d values. So, by using the peak with Miller indices 311, a blue diffraction line shift of $\Delta 2\theta = 28.58^\circ$ (S_2) – 28.64° (S_1) = -0.06° ($\Delta d = 3.121\text{\AA}$ (S_2) – 3.114\AA (S_1) = 0.07\AA) are calculated via Bragg's equation. So there is an expansion in the unit cell.

3. 2. Morphology of the materials

Fig. 2 shows the typical FESEM images of the hydrothermally synthesized $\text{Bi}_2\text{Mn}_2\text{O}_7$ nanomaterials. From the typical FESEM images of S_1 , at low magnification in fig. 2 (a and b), we can see that the morphology of

the obtained materials is in rod-like form. At higher magnification in fig. 2 (c and d), it is clear that the materials are composed of rods with different lengths and thicknesses.

Fig. 3 shows the typical FESEM images of the solid state synthesized $\text{Bi}_2\text{Mn}_2\text{O}_7$ nanomaterials. From the typical FESEM images of S_2 , at low magnification in fig. 3 (a and b) we can see that the morphology of the obtained materials is a mixture of rod and spherical particle forms. At higher magnification in fig. 3 (c and d), it is clear that the materials are composed of rods with different lengths and thicknesses.

Fig. 4 shows the TEM images of the obtained materials via hydrothermal method. It shows that the structure of the materials is rod like that is in agreement with those of fig. 2. Fig. 4 (b and c) shows that the thicknesses of the rod structures are between 60–150 nm (fig. 4b) and 84 nm (fig. 4c). With high magnification in fig. 4 f, the thickness of the material was observed to be about 73 nm.

Fig. 5 shows the TEM images of the obtained materials via hydrothermal method. It shows that the structure of the material is a mixture of rod and particle like, which is in agreement with those of in fig. 3. Fig. 5 (a-c) shows that the thickness of the rod structure is about 240 nm and fig. 5 (d-f) shows that the particle size is about 41 nm.

3. 3. BET and BJH texture analysis

The synthesized powders were characterized in

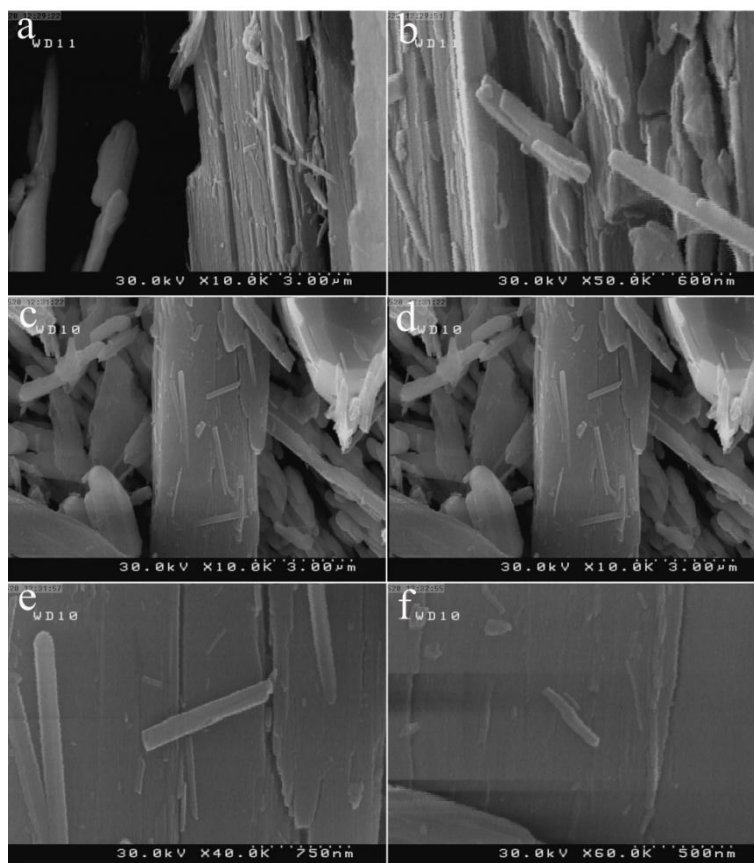


Fig. 2. SEM images of the hydrothermally synthesized $\text{Bi}_2\text{Mn}_2\text{O}_7$ nanomaterials in 1M NaOH solution

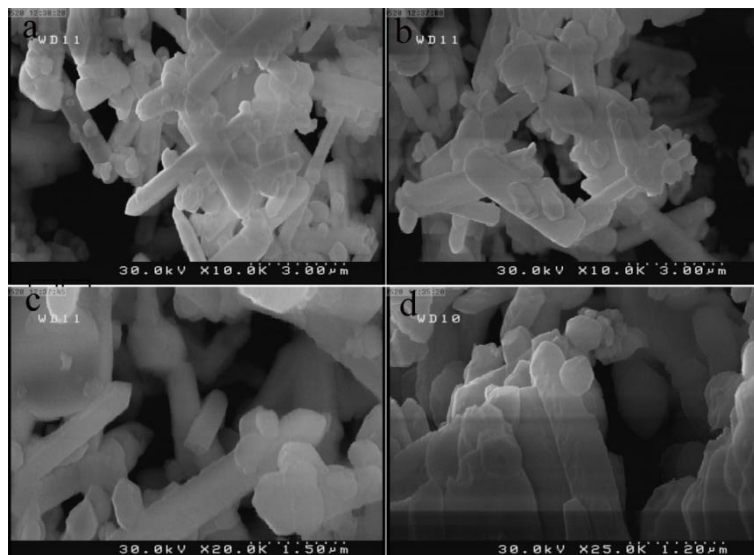


Fig. 3. SEM images of the solid state synthesized $\text{Bi}_2\text{Mn}_2\text{O}_7$ nanomaterials at 550 °C for 8h

terms of their surface area, average pore size and average pore volume. Prior to the N_2 -physical adsorption measurement, the samples were degassed at 150 °C for 120 min in the nitrogen atmosphere. So, the specific

surface area (S_{BET}) of the obtained materials was determined with adsorption-desorption isotherms of N_2 at 77 K. The surface area, pore volume, and average pore diameter of the synthesized materials are summarized in

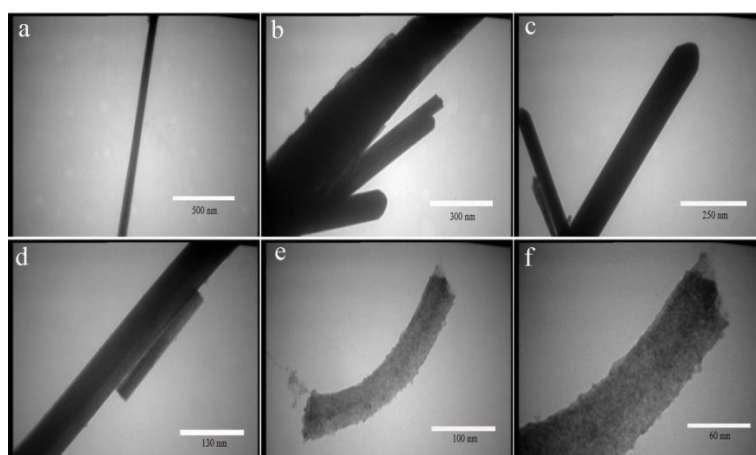


Fig. 4. TEM images of the hydrothermally synthesized $\text{Bi}_2\text{Mn}_2\text{O}_7$ nanomaterials after 48h at 180°C

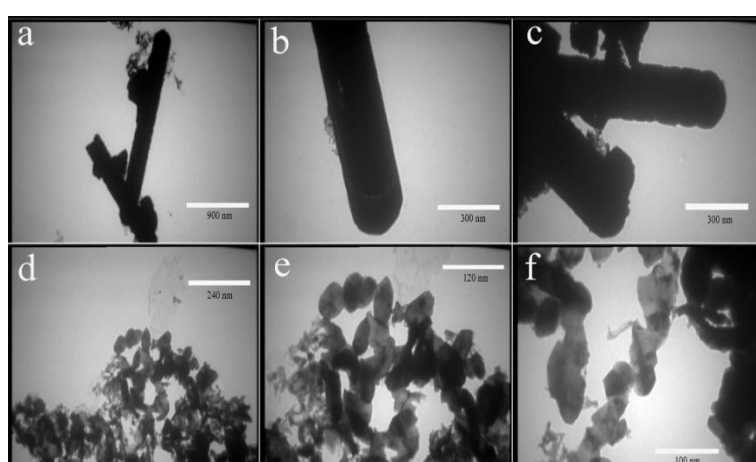


Fig. 5. TEM images of the solid state synthesized $\text{Bi}_2\text{Mn}_2\text{O}_7$ nanomaterials after 48h at 550°C

Table 1. BET data for $\text{Bi}_2\text{Mn}_2\text{O}_7$ showing the textural properties of the obtained materials

Sample	BET surface area (m^2g^{-1})	Pore size (\AA)	Pore volume (cm^3g^{-1})	Average particles size (nm)
S ₁	0.35	126.11	0.002	6954
S ₂	0.74	139.06	0.003	8133

Table 1. It can be seen that the average surface area and pore volumes are about $0.35 \text{ m}^2\text{g}^{-1}$ and $0.002 \text{ cm}^3\text{g}^{-1}$ for S₁ and 0.74 and $0.003 \text{ cm}^3\text{g}^{-1}$ for S₂, respectively. Also, for samples S₁ and S₂, the average nanoparticles sizes were measured as 6954 and 8133 nm, respectively. Table 2 shows the textural properties of the as-prepared materials. The data summarized in this table show that the specific surface area of the pores of the S₂ sample is larger than that of S₁ and the pore width and pore volume of S₂ is larger than that of S₁. So, the investigated results of the BET and BJH measurements suggest that the surface area of S₂ is larger than

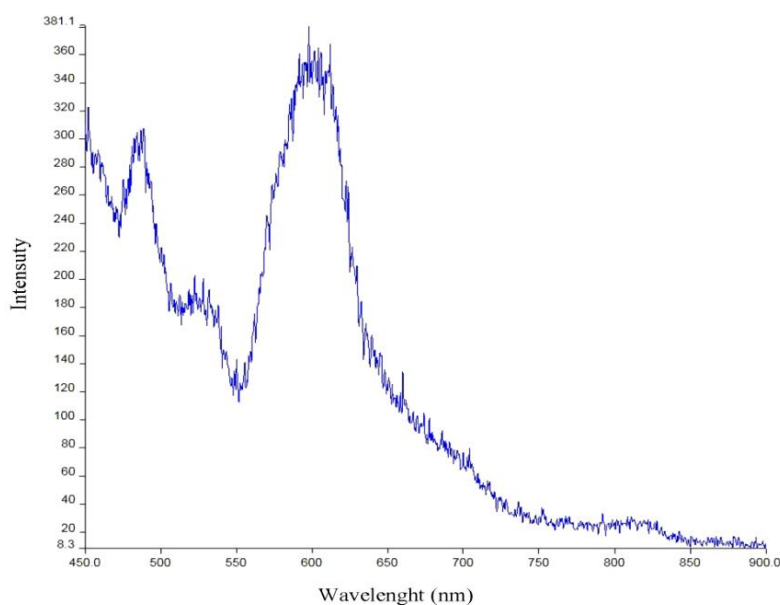
that of S₁. It also shows that by changing the reaction method to solid state, the average particle sizes are larger than those of hydrothermal method that is in good agreement with the FESEM images.

3. 4. Optical Properties

Fig. 6 represents the room-temperature emission spectra of the as-synthesized materials under excitation at 200 nm. Strong broad emission bands at 400-650 nm are observed for samples 1 and 2, respectively. These peaks can be related to Bi-O transitions [14, 15]. The shoulder observed at 650-720 nm can be

Table 2. BJH data for $\text{Bi}_2\text{Mn}_2\text{O}_7$ showing the textural properties of the obtained materials

Property	S_1	S_2
BJH adsorption cumulative surface area of pores between 17 and 3000Å width	0.31 m^2g^{-1}	0.34 m^2g^{-1}
BJH adsorption cumulative volume of pores between 17 and 3000Å width	0.003 cm^3g^{-1}	0.004 cm^3g^{-1}
BJH adsorption average pore width (4V/A)	71nm	69 nm

**Fig. 6.** Photoluminescence spectrum of the hydrothermally synthesized $\text{Bi}_2\text{Mn}_2\text{O}_7$ nanomaterials ($\lambda_{\text{ex}} = 200 \text{ nm}$)

attributed to d-d transitions in Mn cations [16].

4. Conclusion

In this work, $\text{Bi}_2\text{Mn}_2\text{O}_7$ nanomaterials were synthesized via hydrothermal and solid state methods. The PXRD patterns showed that the synthesis was successful. FESEM images showed that the as-synthesized materials are in a rod like and a mixture of rod-particle structures for hydrothermal and solid state methods, respectively. The BET-BJH measurements showed that by changing the reaction method to solid state, the average particle sizes were larger, which shows good agreement with those of the TEM images.

Acknowledgements

The authors express their sincere thanks to Dr. Murat Sertkol from Low Temperature Laboratory Department of Physics, Istanbul Technical University, for performing Rietveld Analysis and interpretation of the data.

References

1. N. Sharma, G. V. SubbaRao, B. V. R. Chowdhuri, "Anodic properties of tin oxides with pyrochlore structure for lithium ion batteries", *J. Power Sources.*, Vol. 159, 2006, pp. 340–344.
2. B. P. Mandal, N. Garg, S. M. Sharma, A. K. Tyagi, "Preparation, XRD and Raman spectroscopic studies on new compounds $\text{Re}_2\text{Hf}_2\text{O}_7$ (RE=Dy, Ho, Er, Tm, Lu, Y): Pyrochlores or defect-fluorite?", *J. Solid State Chem.*, Vol. 179, 2006, pp. 1990–1994.
3. K. Li, T. Zhang, H. Wang, H. Yan, "Low-temperature synthesis and structure characterization of the series $\text{Y}_{2-\delta}\text{Bi}_\delta\text{Sn}_2\text{O}_7$ ($\delta = 0-2.0$) nanocrystals", *J. Solid State Chem.*, Vol. 179, 2006, pp. 1029–1034.
4. H. L. Zhu, D. R. Yang, L. M. Zhu, D. S. Li, P. H. Chen, G. X. Yu, "Hydrothermal Synthesis and Photoluminescence Properties of $\text{La}_{2-x}\text{Eu}_x\text{Sn}_2\text{O}_7$ ($x=0-2.0$) Nanocrystals", *J. Am. Ceram. Soc.*, Vol. 90, 2007, pp. 3095–3098.
5. K. E. Sickafus, L. Minervini, R. W. Grimes, J. A. Valdez, M. Ishimaru, F. Li, K. J. McClellan,

- T. Hartmann, "Radiation tolerance of complex oxides", *Science.*, Vol. 289, 2000, pp. 748–751.
6. M. Sellami, V. Caignaert, M. Hamdad, A. Belarbi, I. Sari-Mohamed, A. Bahmani, N. Bettahar, "Synthesis and characterization of the new pyrochlore $\text{Bi}_{1.5}\text{Sb}_{1.5-x}\text{Nb}_x\text{MnO}_7$ solid solution", *C. R. Chimie.*, Vol. 14, 2011, pp. 887–890.
 7. A. H. Shaari, W. M. Daud, W. Yusoff, M. Hashim, Z. A. Talib, L. K. Pah, T. B. Ping, "sample preparation and dielectric spectrum equivalent circuits modeling for $\text{Bi}_2\text{Mn}_2\text{O}_7$ ", *Solid State Science and Technology.*, Vol. 15, 2007, pp. 223-228.
 8. K. koga, T. Momai, M. Matsunaga, "composition and properties of pyrochlore-type oxides for air electrode in secondary cells", *ECS Transactions.*, Vol. 11(3), 2008, pp.101-104.
 9. MA. Subramanian, G. Aravamudan, S. Rao, *Prog. Solid State Chem.*, 15 (1983) 55.
 10. K. Ozawa, "Lithium Ion Rechargeable Batteries: Materials, Technology, and New Applications", John Wiley & Sons. Section 3.
 11. M. Sellami, V. Caignaert, M. Hamdad, A. Bekka, N. Bettahar, "Synthesis and characterization of new pyrochlore solid solution $\text{Bi}_{1.5}\text{Sb}_{1.5}\text{Cu}_{1-x}\text{Mn}_x\text{O}_7$ ", *J. Alloys and Compounds.*, Vo. 482, 2009, pp. 13–18.
 12. F. W. Bezerra Lopes, C. P. de Souza, A. M. V. de Morais, J. P. Dallas, J. R. Gavarri, "Determination of $\text{RE}_2\text{Ce}_2\text{O}_7$ pyrochlore phases from monazite–allanite ores", *Hydrometallurgy*, Vol. 97, 2009, pp. 167–172.
 13. Z. Hong-song, W. Yuan, L. Gang, C. Xiao-ge, W. Xin-Li, "Investigation about thermal conductivities of $\text{La}_2\text{Ce}_2\text{O}_7$ doped with calcium or magnesium for thermal barrier coatings", *J. Alloys and Compounds.*, Vol. 537, 2012, pp. 141–146.
 14. J. In, I. Yoon, K. Seo, J. Park, J. Choo, Y. Lee, B. Kim, "Polymorph-Tuned Synthesis of α – and β - Bi_2O_3 Nanowires and Determination of Their Growth Direction from Polarized Raman Single Nanowire Microscopy", *Chem. Eur., J. Vo.* 17, 2011, pp. 1304–1309.
 15. C. Jin, H. Kim, K. Baek, H. W. Kim, C. Lee, "Structure and Photoluminescence Properties of $\text{Bi}_2\text{O}_3/\text{ZnO}$ Coaxial Nanorods", *Journal of the Korean Physical Society*, Vol. 57, No. 6, 2010, pp. 1634-1638.
 16. Y. Zhydachevskii, D. Galanciak, S. Kobayakov, M. Berkowski, A. Kamińska, A. Suchocki, Y. Zakharko, A. Durygin, "Photoluminescence studies of Mn^{4+} ions in YAlO_3 crystals at ambient and high pressure", *Journal of Physics: Condensed Matter* Volume 18 Number 49, 2006, pp. 11385–11396.

